



Synthesis and Characterization of AIE-Active B–N-Coordinated Phenalene Complexes

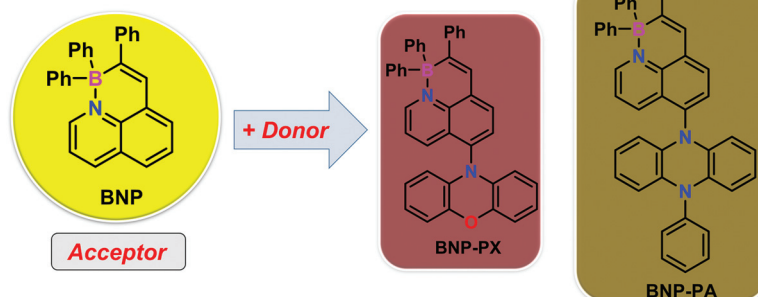
Yubin Fu^a Junzhi Liu^{*b} Zhongbin Wu^{*c} Jan J. Weigand^d Xinliang Feng^{*a} 

^a Center for Advancing Electronics Dresden (cfaed) & Faculty of Chemistry and Food Chemistry, Technische Universität Dresden, 01062 Dresden, Germany
xinliang.feng@tu-dresden.de

^b Department of Chemistry and State Key Laboratory of Synthetic Chemistry, The University of Hong Kong, Pokfulam Road, Hong Kong, China
juliu@hku.hk

^c Department of Materials Science and Engineering, University of Toronto, Toronto, Canada
zhongbin.wu@utoronto.ca

^d Chair of Inorganic Molecular Chemistry, Technische Universität Dresden, 01062 Dresden, Germany



Received: 25.03.2020
Accepted after revision: 13.06.2020

DOI: 10.1055/s-0040-1715564; Art ID: OM-20-0008sc

License terms: 

© 2020. The Author(s). This is an open access article published by Thieme under the terms of the Creative Commons Attribution-NonDerivative-NonCommercial-License, permitting copying and reproduction so long as the original work is given appropriate credit. Contents may not be used for commercial purposes, or adapted, remixed, transformed or built upon. (<https://creativecommons.org/licenses/by-nc-nd/4.0/>).

Abstract Organoboron compounds provide a new line to tune the electronic structures of π -conjugated molecules, which is critical to the development of new organic semiconductor materials. In this work, we demonstrate the synthesis of two novel boron–nitrogen (B–N) coordinated phenalene complexes (**BNP-PX** and **BNP-PA**) by employing BN phenalene (**BNP**) as the acceptor unit and phenoxazine/phenylphenazine groups as the donors. Based on single-crystal X-ray analysis, both **BNP-PX** and **BNP-PA** possess highly twisted conformations with the dihedral angles of 76.6° and 70.5°, respectively. The photophysical properties of **BNP-PX** and **BNP-PA** are elucidated through UV-vis absorption, fluorescence spectroscopy, and theoretical calculations. In addition, **BNP-PX** exhibits a large Stokes shift (8,033 cm^{-1}) and excellent aggregated-induced emission behavior. The red organic light-emitting diode device was fabricated based on compound **BNP-PX**, manifesting its promising application in organic optoelectronic devices.

Key words donor–acceptor, BN-coordinated compounds, large Stokes shift, AIE effect, OLED device

Introduction

π -Conjugated molecules consisting of electron donor (D) and acceptor (A) units have attracted considerable attention due to their enhanced polarizability, narrow energy gap, and

high carrier mobility, which render them actively used in organic semiconductor devices.¹ In particular, the D–A type molecules have made significant progress in the exploitation of organic light-emitting diodes (OLEDs).² Nevertheless, most of the π -conjugated luminophores exhibit weak emission behavior in their aggregated states due to the notorious aggregation-caused emission quenching, which limits the development of efficient OLED devices.³ Toward this end, aggregation-induced emission (AIE) has emerged as an effective strategy to achieve high emission in concentrated solution or even in the solid state.⁴ For instance, the carbon-rich tetraphenylethene and its derivatives have been widely explored to develop high-performance OLEDs.^{3,4} Despite the progress made in recent years, the bottom-up synthesis of AIE-active boron–nitrogen (B–N) containing luminogens remains a challenge.⁵

B–N-doped polycyclic aromatic hydrocarbons (PAHs) exhibit broad absorption and intense fluorescence which can be used as efficient emitters.⁶ In addition, the BN-coordinated unit (B←N) and the C–C unit are also recognized as isoelectronic and isosteric (Figure 1a).⁷ Unlike the nonpolar covalent C–C bond, the B←N bond possesses a large dipole moment and a low bond dissociation energy (Figure 1a).⁸ Accordingly, a B←N unit can serve as a typical kind of Lewis acid/base pair, which has been utilized to synthesize π -conjugated systems with narrow band gaps, high electron affinity, and photochromic properties.^{7,9} For instance, with respect to the unstable phenalene (Figure 1b),¹⁰ upon replacing the C–C unit by a B←N unit, the resultant BN-doped phenalene (**BNP**) exhibits high ambient stability and intense fluorescence.¹¹

Herein, we demonstrate the synthesis of two novel D–A phenalene derivatives (**BNP-PX** and **BNP-PA**; Figure 1c) by

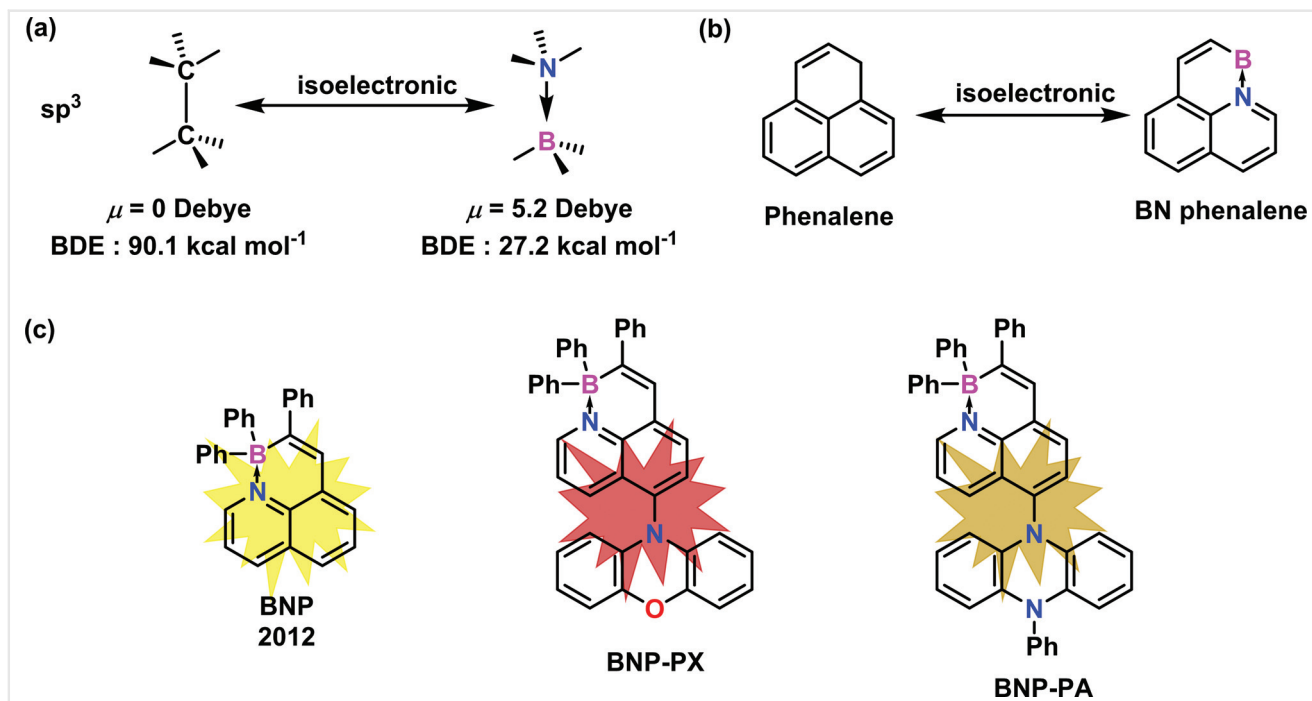


Figure 1 (a) The isoelectronic relationship between B←N coordinated unit and C—C bond. (b) The isoelectronic relationship between phenalene and B←N-doped phenalene; the substituents are omitted for clarity. (c) The design principle toward twisted D-A B←N coordinated phenalene complexes.

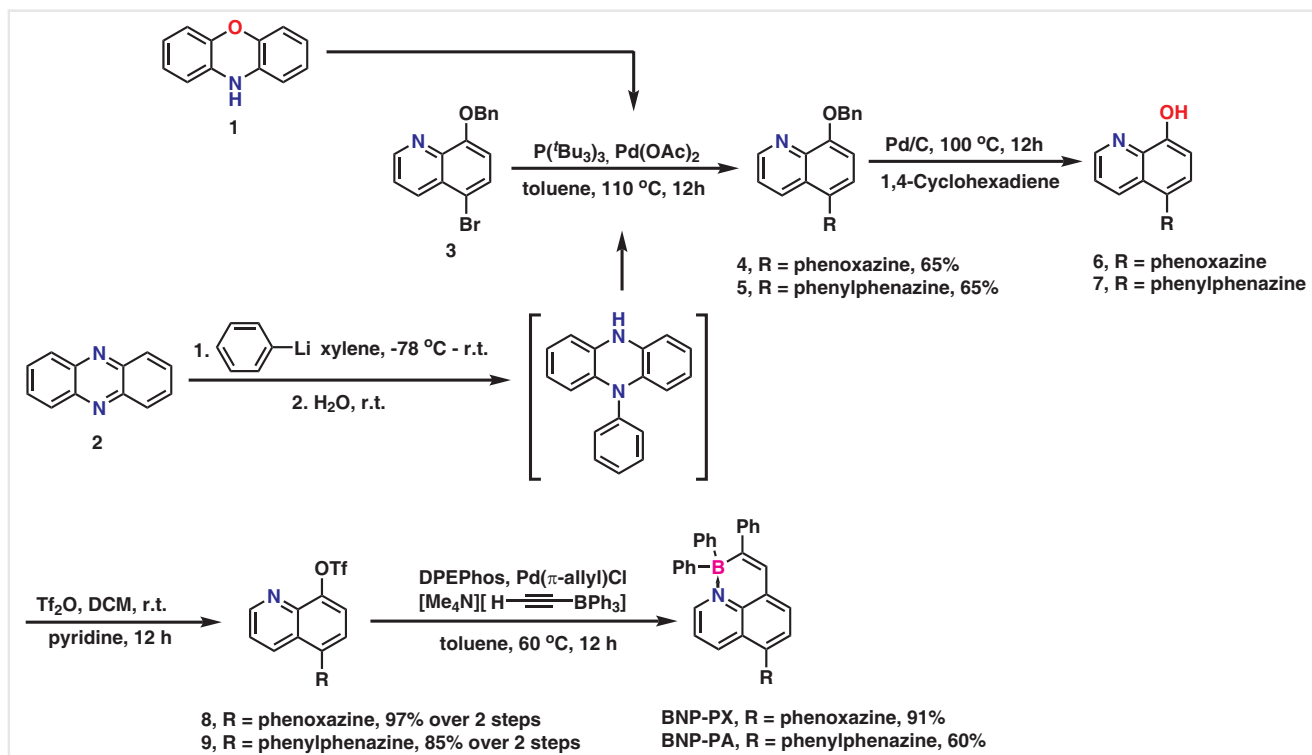
employing **BNP** as the building block. The phenoxazine and phenylphenazine groups in **BNP-PX** and **BNP-PA** not only serve as electron donors but also lead to the highly twisted geometrical conformations, which render the spatial separation of their HOMO and LUMO. Compared to the parent BNP, the frontier orbital energy gaps of **BNP-PX** and **BNP-PA** can be increased by the introduction of the phenoxazine and phenylphenazine substituents. In addition, **BNP-PX** demonstrates the largest Stokes shift (8,033 cm⁻¹) among all the reported B←N coordinated complexes,¹² and exhibits excellent AIE behavior with a quantum yield (Φ) of 0.54 in the solid state. We further fabricated a red OLED device based on **BNP-PX**, revealing its promises in organic optoelectronic devices.

Results and Discussion

The synthetic routes toward **BNP-PX** and **BNP-PA** are depicted in Scheme 1. First, the Buchwald–Hartwig coupling of 8-(benzyloxy)-5-bromoquinoline (**3**) with phenoxazine (**1**) was performed to afford 10-(8-(benzyloxy)quinolin-5-yl)-10*H*-phenoxazine (**4**) in 65% yield. The treatment of **4** with 2 equivalents of 1,4-cyclohexadiene provided 5-(10*H*-phenoxazin-10-yl)quinolin-8-ol (**6**) and the crude product was used without purification in the next step. Subsequently, compound **6** was reacted with trifluoromethanesulfonic anhydride (Tf₂O) to afford 5-(10*H*-phenoxazin-10-yl)quino-

lin-8-yl trifluoromethanesulfonate (**8**) in 97% yield over two steps (Scheme 1).¹³ Next, Pd-induced cyclization of **8** in toluene at 60 °C in the presence of alkynyl(triaryl)borates provided the target compound 10-(1,1,2-triphenyl-1*H*-1λ⁴,10λ⁴-[1,2]azaborinino-[5,6,1-*ij*]quino-lin-6-yl)-10*H*-phenoxazine (**BNP-PX**) in 91% yield. Following a similar synthetic strategy, (*E*)-5-(8-(2-(diphenylboraneryl)-2-phenylvinyl)quinolin-5-yl)-10-phenyl-5,10-dihydrophenazine (**BNP-PA**), in which the substituent phenoxazine in **BNP-PX** was replaced by a phenylphenazine unit, was successfully synthesized starting from compound **3** over four steps (Scheme 1).¹⁴ The targeted compound **BNP-PX** was purified by silica column chromatography and then recrystallized in chloroform/methanol (CHCl₃/MeOH), while **BNP-PA** was obtained by precipitation in MeOH followed by recrystallization in CHCl₃/MeOH. Compounds **BNP-PX** and **BNP-PA** were fully characterized by high-resolution mass spectrometry (HRMS; Figures S39, S40) and ¹H, ¹³C, ¹¹B as well as 2D NMR measurements (Figures S28–S38).

Single crystals of compounds **BNP-PX** and **BNP-PA** were obtained by slow diffusion of a chloroform/methanol mixed solution. **BNP-PX** crystallizes in the monoclinic space group P2₁/c and shows an edge-on twisted geometry (Figure 2a, b). Due to the different rotation angles between the BNP and phenoxazine group (R1), two different conformational isomers (**BNP-PXa** and **BNP-PXb** in Figure 2a, b) are found in the solid state of **BNP-PX**. The bond length of B1–N1 (1.642 Å in **BNP-PXa** and 1.643 Å in **BNP-PXb**; Figure 2a, b)



Scheme 1 Synthetic routes toward compounds **BNP-PX** and **BNP-PA**.

is a typical B←N coordination bond (1.6–1.7 Å),^{5a,15} which is similar to that of reported **BNP** (Figure S1).¹¹ Besides, the dihedral angles of C11–N1–B1–C10 in **BNP-PXa** and **BNP-PXb** are 7.3° and 1.7° (Figure 2a, b), respectively, indicating the nearly planar geometry of the BNP core. Interestingly, the dihedral angles between the BNP and phenoxazine group (C4–C5–N2–C30) in **BNP-PXa** and **BNP-PXb** are 76.6° and 68.0° (Figure 2a, b), respectively. As shown in Figure 2d, **BNP-PX** displays a slipped stack mode with a π – π stacking distance of 3.17 Å (**BNP-PXa**) and 3.45 Å (**BNP-PXb**), respectively, which are shorter than the sum of the van der Waals radii (3.60 Å).¹⁶ Similar to **BNP-PX**, **BNP-PA** also stacks in the monoclinic space group $P2_1/c$ and adopts a twisted geometry (Figure 2c). Although the size of the phenylphenazine group (R2) is comparable to that of the phenoxazine group (R1), only one conformation (Figure 2c) was found in the single-crystal structure of **BNP-PA**. This is possibly due to the existence of an additional phenyl unit in R2, which increases the rotational energy between the R2 and BNP. The bond length of B1–N1 (1.638 Å) in **BNP-PA** is slightly shorter than those of **BNP** and **BNP-PX**. Moreover, the dihedral angle of C7–C6–N2–C41 in **BNP-PA** is 70.5° (Figure 2c), and there is no obvious π – π interaction in the stacking mode of **BNP-PA** (Figure 2e).

The UV-vis absorption and fluorescence spectra of **BNP-PX** and **BNP-PA** in anhydrous toluene solution are presented in Figure 3a. **BNP-PX** displays a maximum absorption peak

at 424 nm, with a bathochromic shift of 7 nm compared with **BNP** (Figure S52 and Table S3). Based on the time-dependent density functional theory (TD-DFT) calculations, this absorption peak of **BNP-PX** can be attributed to the HOMO–1→LUMO transition (Figure S60) and belongs to the local excitation (LE) from the core of BNP according to the corresponding orbital plots (Figure S57). In addition, a weak shoulder absorption at a longer wavelength of **BNP-PX** (450 nm; Figure 3b) was also observed, which is owing to the intramolecular charge transfer (ICT) from the donor phenoxazine group to the acceptor BNP on the basis of measured negative solvatochromic effect^{5a,17} (Figure S41 and Table S2) and TD-DFT calculations (the HOMO→LUMO transition; Figures S60 and S57). The blue shift of the absorption peak with the increased polarity of the solvent (Figure S41) suggests that the ground state of **BNP-PX** is more polar than its excited state, which is consistent with the molecular donor–acceptor (D–A) structure.^{5a,17} For compound **BNP-PA**, a similar absorption peak at $\lambda_{\text{max}} = 424$ nm was observed. According to the TD-DFT calculations, this peak can be assigned to the HOMO–1→LUMO transition (Figure 3a) and also belongs to the LE from the BNP. In addition, there is a broad absorption from 500 to 700 nm for **BNP-PA** (maximum peak at 581 nm; Figure 3b), because of the ICT effect from the donor phenylphenazine group to the acceptor BNP based on the negative solvatochromic effect¹⁷ investigation (Figure S42) and TD-DFT calculations (the

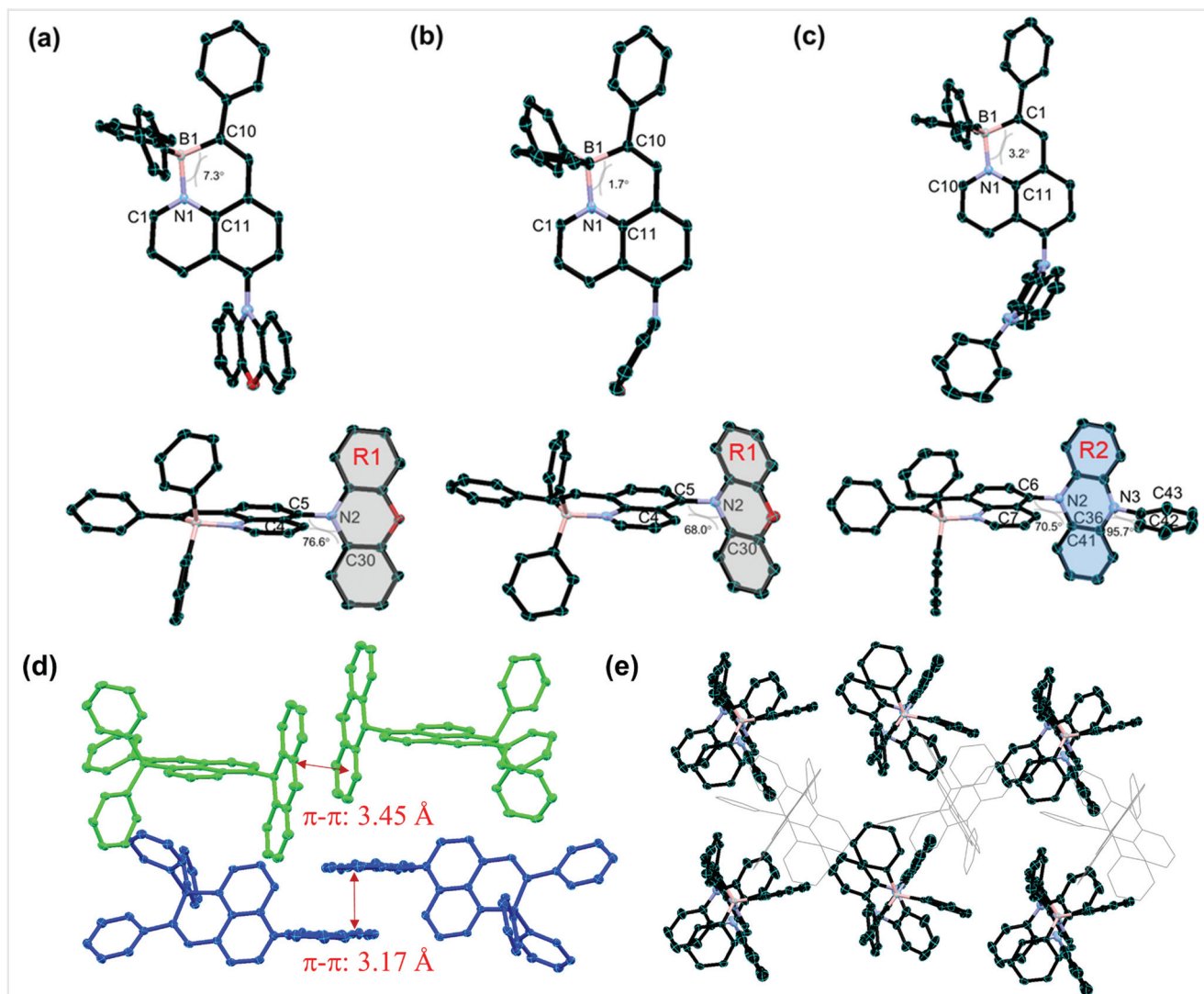


Figure 2 (a, b) Top and side views of single-crystal structure of **BNP-PX** (isomer **BNP-PXa** and **BNP-PXb**). (c) Top and side views of single-crystal structure of **BNP-PA**. (d) Crystal packing of **BNP-PX**, blue: isomer **BNP-PXa**, green: isomer **BNP-PXb**. (e) Crystal packing of **BNP-PA**. 50% probability of thermal ellipsoids; colors: black, carbon; blue, nitrogen; pink, boron; R1: phenoxazine group; R2: phenylphenazine group. Hydrogen atoms are omitted for clarity.

HOMO→LUMO transition; Figures S61 and S58). **BNP-PA** displays a stronger HOMO–LUMO absorption than **BNP-PX** (Figure 3a, b), this is due to the strong electron-donating character of the sp^3 -hybridized phenylphenazine group than that of the phenoxazine unit. Moreover, the weak HOMO–LUMO absorptions of **BNP-PA** and **BNP-PX** are also observed in different solvents (Figures S41 and S42), which are well supported by the TD-DFT calculations. The fluorescence spectra of **BNP-PX** show a maximum emission peak at 643 nm (excited at 424 nm) with a Stokes shift of $8,033\text{ cm}^{-1}$ in toluene (Figure 3c), exhibiting the largest Stokes shift among all the reported B–N-coordinated complexes.¹² However, two maximum peaks (around 460 and 525 nm) with an additional shoulder (around 675 nm) in the emission spectra of **BNP-PX** in dichloromethane (DCM),

THF, and DMF were observed (Figure S43), this is likely attributable to the existence of the twisted ICT.¹⁸ For compound **BNP-PA**, the maximum emission peak at 518 nm can be observed in toluene (excited at 424 nm). Moreover, **BNP-PA** demonstrated a positive solvatochromism of the emission spectra (Figure S44), which may due to the fact that the interaction of **BNP-PA** with different polar solvents is mostly stabilized by the local excited states (as predicted by the TD-DFT calculations).¹⁹ In addition, no emission spectra of **BNP-PA** was observed after excitation at ca. 600 nm in different solvents (Figure S45), indicating that the emission spectra of **BNP-PA** (Figure 3c) mainly came from the second excited state (the HOMO-1→LUMO excitation, which was predicted by TD-DFT calculations). The solution quantum yield (QY) of **BNP** is estimated to be

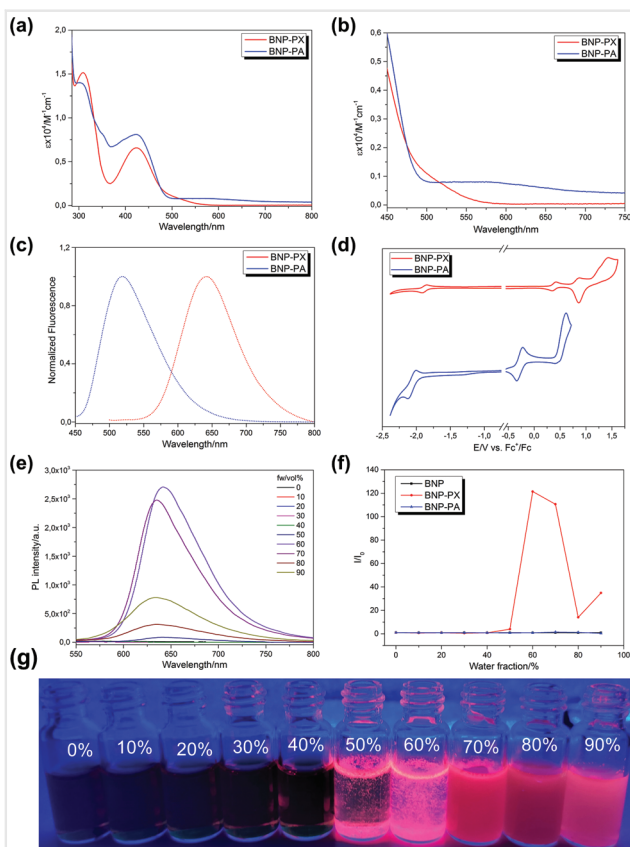


Figure 3 (a) UV-vis absorption spectra of **BNP-PX** and **BNP-PA** in toluene (concentration: 1×10^{-5} M). (b) The locally enlarged UV-vis spectra. (c) Fluorescence spectra of **BNP-PX** and **BNP-PA** in toluene (concentration: 1×10^{-5} M). (d) Cyclic voltammograms of **BNP-PX** and **BNP-PA** measured in CH_2Cl_2 (0.1 M $n\text{-Bu}_4\text{NPF}_6$) at the scan rate of 0.1 V/s. (e) Fluorescence spectra of **BNP-PX** in THF – water mixtures (8.0×10^{-4} M, excited at 424 nm) with varied volumetric fractions (f_w) of water. (f) The fluorescence intensity ratios (I/I_0) of **BNP**, **BNP-PX**, and **BNP-PA** in different fractions of water (I_0 is the fluorescence intensity of **BNP**, **BNP-PX**, and **BNP-PA** in THF). (g) The digital photo of **BNP-PX** in THF – water mixtures under UV light (8.0×10^{-4} M, excited at 365 nm).

0.93 (fluorescein as reference; Table S3). In contrast, the solution QY of **BNP-PX** and **BNP-PA** is estimated to be 0.03 and 0.01 in toluene (Rhodamine 101 and fluorescein as reference; Table S3), respectively. While the solid-state QY of **BNP-PX** is 0.54 based on the measurement by an integral sphere. Such low solution QY of **BNP-PX** is possibly due to the free intramolecular motions between the BNP and phenoxazine group in dilute solvents.²⁰ Furthermore, the fluorescence behavior of **BNP-PX** in THF–water solvents with different water volume fractions (f_w) was recorded. As shown in Figure 3 (e, f), the fluorescence spectra of **BNP-PX** displayed an almost flat line in pure THF solution. Interestingly, when the water fraction was more than 40% (f_w), the fluorescence intensity of **BNP-PX** increased sharply and reached to the highest intensity at 60% (f_w) (Figure 3f, g). Afterwards, it gradually decreased upon

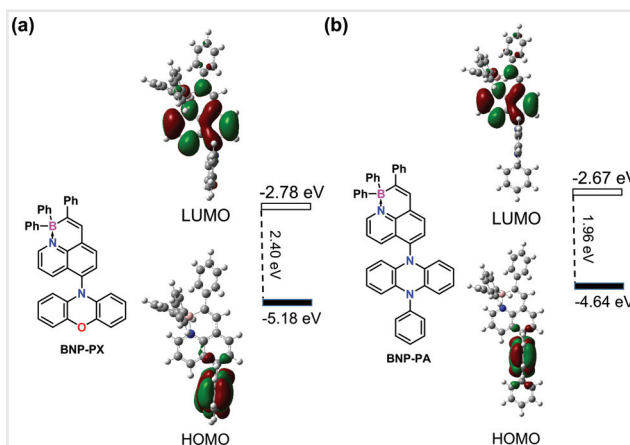


Figure 4 Calculated molecular orbitals and energy diagrams of (a) **BNP-PX** and (b) **BNP-PA**.

increasing the fractions of water. These results strongly suggest a typical solvent-dependent AIE character for **BNP-PX**. In contrast, there was no AIE response for **BNP** and **BNP-PA** under the same conditions (Figures 3f, S50, and S51). According to the concentration-dependent absorption and fluorescence spectra (Figure S47), there is no obvious excimerformation of **BNP-PX** under high concentrations. According to the temperature-dependent absorption and fluorescence spectra (Figure S48), the intensity of the HOMO–LUMO absorption and the maximum emission peak of **BNP-PX** increased with temperature. Thus, we consider that the unique AIE response for **BNP-PX** might be caused by a restriction of intramolecular motion mechanism,²⁰ where the free rotational motion of the phenoxazine group in **BNP-PX** is limited in the aggregated state, resulting in the cut off of nonradiative transition and intense luminescence.²¹ In addition, **BNP-PX** showed similar solvent-dependent AIE behavior in the THF–hexane solvent (Figure S49).

The electrochemical behaviors of **BNP-PX** and **BNP-PA** in anhydrous DCM were investigated by means of cyclic voltammetry (CV) as depicted in Figure 3d. **BNP-PX** displayed a reversible reduction process at the half-wave potential of -1.88 V vs. Fc^+/Fc (Figure 3d). In addition, one reversible, one quasi-reversible, and one irreversible oxidation processes were observed with a half-wave potential at 0.38, 0.87, and 1.28 V vs. Fc^+/Fc (Figure 3d), respectively. For **BNP-PA**, one quasi-reversible reduction process was identified with a half-wave potential at -2.06 V vs. Fc^+/Fc (Figure 3d). Moreover, **BNP-PA** exhibited one reversible and one irreversible oxidation processes with a half-wave potential at -0.28 and 0.52 V vs. Fc^+/Fc (Figure 3d), respectively. However, under high potential (>0.8 V vs. Fc^+/Fc), the CV curves of **BNP-PA** became complex owing to its low electrochemical stability (Figure S54). Accordingly, the LUMO energy levels are

estimated to be -2.92 and -2.74 eV for **BNP-PX** and **BNP-PA**, respectively (Table S3). On the basis of their optical energy gaps obtained from their absorption edges, the HOMOs of **BNP-PX** and **BNP-PA** are derived to be -5.42 and -5.22 eV, respectively (Table S3). The HOMO and LUMO energy levels of **BNP-PX** and **BNP-PA** are obviously higher than that of **BNP** (HOMO: -6.06 eV; LUMO: -3.50 eV), manifesting the important role of the integrated donor moieties (phenoxazine and phenylphenazine groups). In addition, the experimental results are well supported by the DFT calculations (Figure 4 and Table S3). The HOMOs in **BNP-PX** and **BNP-PA** are mainly localized on the phenoxazine and phenylphenazine groups due to their electron-donating properties. In contrast, the LUMOs of **BNP-PX** and **BNP-PA** are fully localized over the BNP motif. In comparison with **BNP** (Figure S56), the frontier molecular orbitals of **BNP-PX** and **BNP-PA** are spatially separated, indicating their typical D–A configurations.^{5a,17}

The thermal stability of **BNP-PX** was analyzed by the thermogravimetric analysis (TGA) method under a N_2

atmosphere, as shown in Figure S55. At the beginning of the heating process (25 – 150 °C), the adsorbed water or residual organic solvent is released, resulting in a weight loss of $\sim 2.0\%$. At the temperature range of 150 – 280 °C, there is a weight loss of $\sim 3.0\%$ occurred on the TGA curve, suggesting the decomposition of **BNP-PX**. Accordingly, **BNP-PX** exhibits a decomposition temperature T_d ($T_{d5\%}$, corresponding to 5% weight loss) more than 280 °C, indicating its relatively good thermal stability. To evaluate the electroluminescence (EL) behavior of **BNP-PX** as the emitter in the host–guest and nondoped systems, vacuum-sublimated OLEDs with a configuration of indium tin oxide (ITO)/ MoO_3 (10 nm)/1,1'-bis[4-(di-*p*-tolylamino)phenyl]-cyclohexane (TAPC) (30 nm)/4,4',4''-tri(N-carbazolyl)-triphenylamine (TCTA) (5 nm)/emissive layer/LiF (1 nm)/Al (100 nm) were fabricated, in which MoO_3 , TAPC, and TmPyPB worked as the hole-injection, hole-transporting, and electron-transporting layers, respectively (Figure 5a). In addition, TCTA and LiF were used as the exciton-blocking layer and the electron-injection layer, respectively

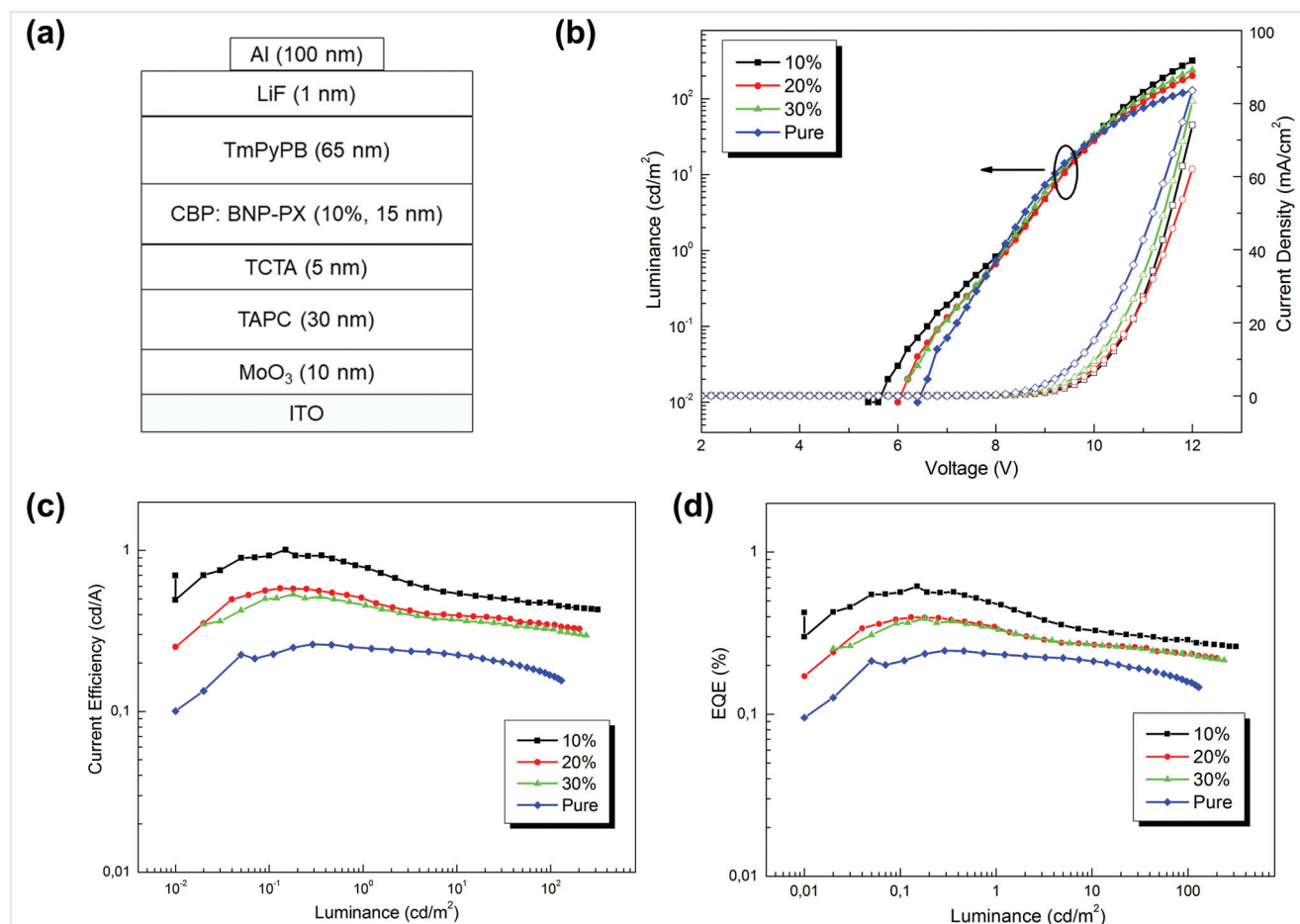


Figure 5 (a) Schematic diagrams of the basic structures of the OLED device based on **BNP-PX**. (b) Current density – voltage – luminance (J – V – L) characteristics. (c) Current efficiency (CE) – luminance characteristics. (d) External quantum efficiency (EQE) – luminance characteristics.

(Figure 5a). As shown in Figure 5 (b, c), the turn-on voltage of the devices is around 6.0 V, and the maximum brightness is 317 cd/m². Varying the driving voltages of 6.0, 8.0, and 10.0 V, the devices show very small spectra shifts (Figure S62). The EL spectra and color coordinates of these devices show a small variation from low-to-high driving voltages, implying the efficient energy transfer from the host to the guest. Among the devices fabricated, the optimized device exhibits a maximum external quantum efficiency (EQE) of 0.6% and a maximum current efficiency of 1.0 cd/A (Figure 5d).

Conclusions

In conclusion, we report the synthesis of two novel BN-coordinated phenalene derivatives containing D–A structures (**BNP-PX** and **BNP-PA**). Single-crystal analysis together with the DFT calculations reveals that both **BNP-PX** and **BNP-PA** possess highly twisted geometries, which render the spatial separation of the HOMO and LUMO distributions. By introduction of the phenoxazine and phenylphenazine substituents, the frontier orbital energy levels of **BNP-PX** (HOMO: –5.42 eV; LUMO: –2.92 eV) and **BNP-PA** (HOMO: –5.22 eV; LUMO: –2.74 eV) are increased compared with the parent **BNP** (HOMO: –6.06 eV; LUMO: –3.50 eV). In addition, **BNP-PX** demonstrates excellent AIE effect and mega-large Stokes shift (8,033 cm^{–1}) among all the reported BN-coordinated compounds. Furthermore, the OLED device was fabricated based on **BNP-PX** with the EQE up to 0.6%. This work reported herein demonstrates that the B–N-coordinated PAHs with donor–acceptor configurations can be generally interesting for optoelectronic devices.

Funding Information

We thank the European Union's Horizon 2020 research and innovation program under grant agreement No. 696656 (Graphene Flagship Core2), ERC Grant on T2DCP, the German Research Foundation (DFG) within the Cluster of Excellence "Center for Advancing Electronics Dresden (cfaed)" and EnhanceNano (No. 391979941) as well as the European Social Fund and the Federal State of Saxony (ESF Project "GRAPHD", TU Dresden) for financial support. J. Liu is grateful for the startup funding from The University of Hong Kong and the funding support from ITC to the SKL.

Acknowledgments

We thank Mr. Mingchao Wang (Technische Universität Dresden) for HR-MS measurement. We thank Prof. Sebastian Reineke and Dr. Yungui Li (IAPP, Technische Universität

Dresden) for solid quantum yield measurement. We thank the Center for Information Services and High Performance Computing (ZIH) at TU Dresden for generous allocations of computing resources.

Supporting Information

Supporting information for this article is available online at <https://doi.org/10.1055/s-0040-1715564>.

References and Notes

- (1) (a) Wu, Y.; Zhu, W. *Chem. Soc. Rev.* **2013**, *42*, 2039. (b) Zhang, J.; Xu, W.; Sheng, P.; Zhao, G.; Zhu, D. *Acc. Chem. Res.* **2017**, *50*, 1654. (c) Zhang, J.; Jin, J.; Xu, H.; Zhang, Q.; Huang, W. *J. Mater. Chem. C Mater. Opt. Electron. Devices* **2018**, *6*, 3485. (d) Zhang, G.; Zhao, J.; Chow, P. C. Y.; Jiang, K.; Zhang, J.; Zhu, Z.; Zhang, J.; Huang, F.; Yan, H. *Chem. Rev.* **2018**, *118*, 3447. (e) Li, Y.; Liu, J.-Y.; Zhao, Y.-D.; Cao, Y.-C. *Mater. Today* **2017**, *20*, 258. (f) Geng, H.; Zheng, X.; Shuai, Z.; Zhu, L.; Yi, Y. *Adv. Mater.* **2015**, *27*, 1443. (g) Richter, M.; Fu, Y.; Dmitrieva, E.; Weigand, J. J.; Popov, A.; Berger, R.; Liu, J.; Feng, X. *ChemPlusChem* **2019**, *84*, 613.
- (2) (a) Cao, X.; Zhang, D.; Zhang, S.; Tao, Y.; Huang, W. *J. Mater. Chem. C Mater. Opt. Electron. Devices* **2017**, *5*, 7699. (b) Ledwon, P. *Org. Electron.* **2019**, *75*, 105422. (c) Tao, Y.; Yuan, K.; Chen, T.; Xu, P.; Li, H.; Chen, R.; Zheng, C.; Zhang, L.; Huang, W. *Adv. Mater.* **2014**, *26*, 7931.
- (3) (a) Hong, Y.; Lam, J. W. Y.; Tang, B. Z. *Chem. Commun. (Camb.)* **2009**, (29):4332. (b) Hong, Y.; Lam, J. W. Y.; Tang, B. Z. *Chem. Soc. Rev.* **2011**, *40*, 5361.
- (4) (a) Li, H.; Li, B. S.; Tang, B. Z. *Chem. Asian J.* **2019**, *14*, 674. (b) Wang, H.; Zhao, E.; Lam, J. W. Y.; Tang, B. Z. *Mater. Today* **2015**, *18*, 365.
- (5) (a) Fu, Y.; Qiu, F.; Zhang, F.; Mai, Y.; Wang, Y.; Fu, S.; Tang, R.; Zhuang, X.; Feng, X. *Chem. Commun. (Camb.)* **2015**, *51*, 5298. (b) Shen, P.; Zhuang, Z.; Zhao, Z.; Tang, B. Z. *J. Mater. Chem. C Mater. Opt. Electron. Devices* **2018**, *6*, 11835. (c) Wan, W.-M.; Tian, D.; Jing, Y.-N.; Zhang, X.-Y.; Wu, W.; Ren, H.; Bao, H.-L. *Angew. Chem. Int. Ed.* **2018**, *57*, 15510.
- (6) (a) Wang, X.; Zhang, F.; Liu, J.; Tang, R.; Fu, Y.; Wu, D.; Xu, Q.; Zhuang, X.; He, G.; Feng, X. *Org. Lett.* **2013**, *15*, 5714. (b) Zhang, W.; Zhang, F.; Tang, R.; Fu, Y.; Wang, X.; Zhuang, X.; He, G.; Feng, X. *Org. Lett.* **2016**, *18*, 3618. (c) Zhang, W.; Fu, Y.; Qiang, P.; Hunger, J.; Bi, S.; Zhang, W.; Zhang, F. *Org. Biomol. Chem.* **2017**, *15*, 7106. (d) Wang, X.; Zhang, F.; Gao, J.; Fu, Y.; Zhao, W.; Tang, R.; Zhang, W.; Zhuang, X.; Feng, X. *J. Org. Chem.* **2015**, *80*, 10127. (e) Wang, X.; Zhang, F.; Schellhammer, K. S.; Machata, P.; Ortmann, F.; Cuniberti, G.; Fu, Y.; Hunger, J.; Tang, R.; Popov, A. A.; Berger, R.; Müllen, K.; Feng, X. *J. Am. Chem. Soc.* **2016**, *138*, 11606. (f) Fu, Y.; Zhang, K.; Dmitrieva, E.; Liu, F.; Ma, J.; Weigand, J. J.; Popov, A. A.; Berger, R.; Pisula, W.; Liu, J.; Feng, X. *Org. Lett.* **2019**, *21*, 1354.
- (7) (a) Dou, C.; Ding, Z.; Zhang, Z.; Xie, Z.; Liu, J.; Wang, L. *Angew. Chem. Int. Ed.* **2015**, *54*, 3648. (b) Wang, T.; Dou, C.; Liu, J.; Wang, L. *Chemistry* **2018**, *24*, 13043.
- (8) (a) Grant, D. J.; Dixon, D. A. *J. Phys. Chem. A* **2006**, *110*, 12955. (b) Blanksby, S. J.; Ellison, G. B. *Acc. Chem. Res.* **2003**, *36*, 255.
- (9) (a) Mukundam, V.; Sa, S.; Kumari, A.; Das, R.; Venkatasubbaiah, K. *J. Mater. Chem. C Mater. Opt. Electron. Devices* **2019**, *7*, 12725.

- (b) Qiu, F.; Zhang, F.; Tang, R.; Fu, Y.; Wang, X.; Han, S.; Zhuang, X.; Feng, X. *Org. Lett.* **2016**, *18*, 1398. (c) Morgan, M. M.; Nazari, M.; Pickl, T.; Rautiainen, J. M.; Tuononen, H. M.; Piers, W. E.; Welch, G. C.; Gelfand, B. S. *Chem. Commun. (Camb.)* **2019**, 55, 11095. (d) Pammer, F.; Schepper, J.; Glöckler, J.; Sun, Y.; Orthaber, A. *Dalton Trans.* **2019**, 48, 10298.
- (10) Uchida, K.; Kubo, T. *J. Synth. Org. Chem. Jpn.* **2016**, *74*, 1069.
- (11) Ishida, N.; Narumi, M.; Murakami, M. *Helv. Chim. Acta* **2012**, *95*, 2474.
- (12) (a) Ren, X.; Zhang, F.; Luo, H.; Liao, L.; Song, X.; Chen, W. *Chem. Commun. (Camb.)* **2020**, 56, 2159. (b) Araneda, J. F.; Piers, W. E.; Heyne, B.; Parvez, M.; McDonald, R. *Angew. Chem. Int. Ed.* **2011**, *50*, 12214.
- (13) **Synthetic procedure for compound BNP-PX:** In a 50 mL one-necked flask, compound **8** (153.5 mg, 0.32 mmol), alkynylborate (120.9 mg, 0.35 mmol), DPEPhos (16.3 mg, 0.03 mmol) and Pd(π -allyl)Cl (17.2 mg, 0.047 mmol) were charged under argon atmosphere. After three times vacuum-argon operation, degassed toluene (10 mL) was added into the flask under argon. Then the mixture was stirred at 60 °C for 12 h. Afterwards, the reaction mixture was concentrated under reduced pressure. The residue was then purified by chromatography on silica gel (CH₂Cl₂/iso-hexane = 1/1) to give product as red powder (167.8 mg, 91%). ¹H NMR (300 MHz, CD₂Cl₂) δ 8.87 (dd, J = 5.5, 1.5 Hz, 1H), 8.67 (dd, J = 8.4, 1.5 Hz, 1H), 7.91 (d, J = 7.8 Hz, 1H), 7.79 (d, J = 7.7 Hz, 1H), 7.47 (dd, J = 8.4, 5.5 Hz, 1H), 7.38 (d, J = 1.5 Hz, 2H), 7.35 (d, J = 1.3 Hz, 2H), 7.24 (s, 1H), 7.21 (t, J = 1.7 Hz, 1H), 7.18 (d, J = 1.5 Hz, 2H), 7.16 (s, 2H), 7.14 (dd, J = 3.2, 1.5 Hz, 2H), 7.12 (s, 3H), 7.10 (dd, J = 4.1, 2.1 Hz, 1H), 6.78 (dd, J = 7.9, 1.6 Hz, 2H), 6.71 (td, J = 7.6, 1.4 Hz, 2H), 6.58 (td, J = 7.7, 1.6 Hz, 2H), 5.86 (d, J = 1.4 Hz, 1H), 5.84 (d, J = 1.4 Hz, 1H). ¹¹B NMR (96 MHz, CD₂Cl₂) δ 2.20. ¹³C NMR (76 MHz, CD₂Cl₂) δ 153.6, 150.8, 146.1, 144.3, 140.5, 137.4, 134.8, 134.5, 134.2, 133.0, 132.5, 131.2, 128.5, 128.3, 127.8, 127.7, 126.7, 125.8, 125.2, 124.0, 122.6, 122.5, 116.1, 113.8. HRMS (ACPI, m/z): calcd for C₄₁H₃₀BN₂O⁺ [M + H]⁺ 577.2451, found 577.2447.
- (14) **Synthetic procedure for compound BNP-PA:** In a 50 mL one-necked flask, compound **9** (59.9 mg, 0.11 mmol), alkynylborate (49.8 mg, 0.14 mmol), DPEPhos (13.0 mg, 0.024 mmol) and Pd(π -allyl)Cl (14.4 mg, 0.039 mmol) were charged under argon atmosphere. After three times vacuum-argon operation, degassed toluene (5 mL) was added into the flask under argon. Then the mixture was stirred at 60 °C for 12 h. After cooling down to room temperature, anhydrous methanol (15 mL) was added into the flask and some brown solid precipitated to the bottom. The solid was collected by filtration and then washed by MeOH. The dark brown to black solid (43.0 mg, 60%) can be used directly for further characterization. ¹H NMR (300 MHz, CD₂Cl₂) δ 8.96 (dd, J = 8.4, 1.6 Hz, 1H), 8.92–8.84 (m, 1H), 7.94 (d, J = 7.7 Hz, 1H), 7.85 (d, J = 7.7 Hz, 1H), 7.68 (t, J = 7.6 Hz, 3H), 7.60–7.51 (m, 2H), 7.46 (d, J = 7.7 Hz, 3H), 7.38 (d, J = 1.7 Hz, 2H), 7.35 (s, 2H), 7.25–7.17 (m, 4H), 7.15 (d, J = 5.9 Hz, 3H), 7.12 (d, J = 2.7 Hz, 5H), 6.30 (t, J = 7.5 Hz, 2H), 6.21 (t, J = 7.5 Hz, 2H), 5.71–5.64 (m, 2H), 5.57–5.49 (m, 2H). ¹¹B NMR (96 MHz, CD₂Cl₂) δ –5.37. ¹³C NMR (76 MHz, CD₂Cl₂) δ 150.8, 146.2, 140.9, 140.3, 137.8, 137.0, 136.4, 134.5, 134.5, 134.0, 133.5, 131.8, 131.6, 131.5, 129.3, 128.8, 128.6, 128.3, 127.7, 127.6, 126.6, 125.8, 125.3, 122.5, 121.9, 121.3, 113.2, 112.9. HRMS (ACPI, m/z): calcd for C₄₇H₃₄BN₃⁺ [M]⁺ 651.2846, found 651.2845.
- (15) Berski, S.; Latajka, Z.; Gordon, A. J. *New J. Chem.* **2011**, *35*, 89.
- (16) (a) Janiak, C. *J. Chem. Soc., Dalton Trans.* **2000**, 3885. (b) Hunter, C. A.; Sanders, J. K. M. *J. Am. Chem. Soc.* **1990**, *112*, 5525. (c) Banerjee, A.; Saha, A.; Saha, B. K. *Cryst. Growth Des.* **2019**, *19*, 2245.
- (17) Sun, L.; Zhang, F.; Wang, X.; Qiu, F.; Xue, M.; Tregnago, G.; Cacialli, F.; Osella, S.; Beljonne, D.; Feng, X. *Chem. Asian J.* **2015**, *10*, 709.
- (18) (a) Lin, J. H.; Elangovan, A.; Ho, T. I. *J. Org. Chem.* **2005**, *70*, 7397. (b) Yang, W.; Zhu, W.; Zhou, W.; Liu, H.; Xu, Y.; Fan, J. J. *Fluoresc.* **2012**, *22*, 1383.
- (19) Anandhan, K.; Cerón, M.; Perumal, V.; Ceballos, P.; Gordillo-Guerra, P.; Pérez-Gutiérrez, E.; Castillo, A. E.; Thamotharan, S.; Percino, M. J. *RSC Advances* **2019**, *9*, 12085.
- (20) (a) Mei, J.; Hong, Y.; Lam, J. W. Y.; Qin, A.; Tang, Y.; Tang, B. Z. *Adv. Mater.* **2014**, *26*, 5429. (b) Mei, J.; Leung, N. L. C.; Kwok, R. T. K.; Lam, J. W. Y.; Tang, B. Z. *Chem. Rev.* **2015**, *115*, 11718.
- (21) Kong, Y.-J.; Yan, Z.-P.; Li, S.; Su, H.-F.; Li, K.; Zheng, Y.-X.; Zang, S.-Q. *Angew. Chem. Int. Ed.* **2020**, *59*, 5336.